Application Model of Hyperspectral Technology Based on Novel Spectral Indices for Salinity Assessment in Soil Heritage Sites

Fang Liu[1,2], Yikang Ren[1,2]

1 School of Geomatics and Urban Information, Beijing University of Civil Engineering and Architecture,, Beijing 102612, China-2108570022072@stu.bucea.cn(Y.K.R.),lf@bucea.edu.cn (F.L.)
2 Key laboratory of Modern Urban Surveying and Mapping. National Administration of Surveying, Mapping and Geoinformation,102616,Beijing, China-2108570022072@stu.bucea.cn(Y.K.R.),lf@bucea.edu.cn (F.L.)

KEY WORDS: Spectral index, Fractional Order differential preprocessing, Correlation coefficient, Salt damage

ABSTRACT:

The Dunhuang murals are a precious treasure of China's cultural heritage, yet they have long been affected by salt damage. Traditional methods for detecting salt content are costly, inefficient, and may cause physical harm to the murals. Among current techniques for measuring salt content in murals, hyperspectral remote sensing technology offers a non-invasive , circumventing issues of high costs, low efficiency. Building on this, our study developed a high-spectral feature inversion model for mural phosphate content using Fractional Order Differentiation (FOD), a novel three-band spectral index, and Partial Least Squares Regression (PLSR) algorithm. The specific research contents include: 1) Exploring the absorption mechanism of phosphates and their characteristic bands, combined with the optimal spectral index to construct a univariate linear regression model, providing a basis for rapid quantitative measurement of mural phosphate content. 2) By comparing the accuracy of the PSR and PNDI spectral indices based on the linear regression model, the first six orders of the highest accuracy spectral index were selected as the optimal three-band spectral index combination, used as explanatory variables, with mural plaster electrical conductivity as the response variable, employing the PLSR method to construct the mural phosphate content high-spectral feature inversion model. The study's findings include:1) By comparing the outcomes of different orders of fractional differentiation, it was found that the model performance reached its optimum at a 0.3 order of differentiation for both PSR and PNDI data, with a determination coefficient (R^2) of 0.728. 2) Utilizing PLSR, this study employed the previously determined optimal six-order three-band spectral index combination as explanatory variables, with salt content as the response variable, successfully constructing the high-spectral feature inversion model for mural phosphate content with a determination coefficient (R^2) of 0.815. This provides an effective technical means for monitoring the salt damage conditions of precious cultural heritage such as murals.

1. INTRODUCTION

Ancient mural sites, serving as a vivid annotation of history, not only chronicle the evolution of human civilization but also mirror the levels of production and daily life in ancient societies. In China, the Dunhuang murals, heralded as national treasures of cultural heritage, are world-renowned for their rich themes, exquisite craftsmanship, and unique historical significance. These murals not only depict the religious beliefs, social life, and artistic styles from over a millennium ago but also constitute invaluable resources for the study of cultural exchanges along the ancient Silk Road(Sun, Tongxin, et al., 2023). Regrettably, due to the ravages of time, these murals have suffered from environmental impacts, resulting in fading, efflorescence, erosion by wind and sand, and mold damage. The detachment of the mural pigment layer from its mural plaster base, as well as the separation of the plaster layer from the cliff support layer, gravely diminishes the aesthetic and historical value of these murals (Sharma, et al., 2023). Preserving these murals is tantamount to salvaging a civilization and art on the brink of extinction. Extensive research indicates that changes in the hydrothermal environment are a significant causative factor in the deterioration of mural paintings due to salt crystallization. Among existing methods for salt content analysis in mural samples, Spectrometer Diagnostics stands out as a non-contact, non-destructive technique (Li, D., et al., 2023). When studying salt content in murals, hyperspectral imaging can provide critical information on chemical composition, spatial distribution, quantity estimation, crystallization monitoring, environmental effects, and non-destructive testing, revealing these characteristics through spectral reflection and absorption (Peng, W., et al., 2022; Schodlok, M. C., et al., 2022; Ma, J., et al., 2022).

The utilization of spectral indices constitutes a straightforward and efficacious methodology for measuring surface properties, with band optimization algorithms extensively applied in the development of hyperspectral technology(Zhang, Z., et al 2020). Compared to one-dimensional spectral data, this approach affords a richer spectrum of spectral features, thereby fortifying the correlation between soil properties and spectral characteristics(Noda, I., 2006). For instance, research conducted by Lihan Chen et al(Chen, L., et al 2022)delves into the efficacy of visible-near infrared spectroscopy in estimating the content of heavy metals in soil. Through an analysis of 120 soil samples collected in Xuzhou City, Jiangsu Province, not only were the heavy metal content and spectral characteristics of the samples determined, but attempts were also made to enhance the spectral information of soil heavy metals through fractional order derivative spectral preprocessing methods (FOD) and a novel three-band index, concurrently addressing issues of collinearity and redundancy inherent in hyperspectral data. Jing Yuan et al(Yuan, J., et al 2024) proposed a soil organic matter content estimation method based on an improved Hapke model, anchored in the radiative transfer process of soil reflectance spectra. By transforming reflectance and single scattering albedo, they constructed spectral indices, thus facilitating the remote sensing estimation of soil organic

matter content. According to the aforementioned analyses, spectral indices are capable of effectively capturing the hyperspectral response of soil components, and by expressing them within two-dimensional or multidimensional spectral spaces, they mitigate interference from other soil components in estimation outcomes. Moreover, spectral indices enhance the subtle correlations between bands, simplify model structures, and eliminate redundant information variables. Therefore, applying spectral indices to quantitatively analyze the interactions between characteristic bands of phosphates in mural plaster can significantly enhance the accuracy of phosphate content estimation models. Existing research employing various spectral index combination methods (such as normalization, difference, and ratio) has leveraged hyperspectral data to explore the relationship between soil reflectance and soil components. Compared to dual-band spectral indices, three-band indices incorporate a third band within specific sensitive areas, a processing method that often improves the precision of the estimate, enhances interference resistance, eliminates the saturation phenomenon common to dual-band indices, rendering the estimation of soil components more robust and accurate.

In the process of safeguarding these irreplaceable cultural assets, understanding the phosphate content within mural plaster is crucial for the prevention and treatment of salt damage. Phosphates, under certain hydrothermal conditions, can form dodecahydrates, posing a greater threat to mural cultural heritage compared to common sulfates. Therefore, this study is dedicated to simulating the capillary salt ion adsorption and crystalline erosion degradation processes within the in-situ environment of murals, a method that diverges from traditional laboratory practices of preparing samples with predetermined salt content. This approach more closely mirrors the actual conditions under which murals suffer salt damage, enabling a thorough exploration of the specific impact mechanisms of salts at the microscopic level, thereby providing a more precise and practical scientific basis for mural conservation. Further, by exploring the absorption mechanisms of phosphates and their characteristic bands, and utilizing band optimization algorithms to develop a new three-band spectral index, this study aims to more accurately reflect phosphate content, filling the gap in existing research regarding the precise inversion of phosphate content in its various physical states. This represents a relatively novel endeavor in the field of hyperspectral remote sensing technology, where fractional order differentiation methods offer a more flexible framework capable of capturing finer spectral variations, particularly suited for handling nonlinear and complex physical processes.

2. EXPERIMENT AREA AND SAMPLE PREPARATION

Ancient murals were selected for study due to their distinguished historical value and the characteristic phenomena of salt damage they exhibit. The research site is located at the Mogao Caves in Dunhuang City (approximately 25 km southeast of Dunhuang City, with coordinates at 94.662°E longitude and 40.142°N latitude). Figure 1 illustrates typical types of salt damage to the murals in the research area, including: (a) Plaster Detachment: Partial separation of the plaster layer from the supporting structure, with the detached portion still connected to the support around its periphery. This includes instances where the upper layer of double-layered murals partially detaches from the lower layer. (b) Cracks: Misalignment and cracking phenomena in the murals. (c) Craquelure: Fine network of surface cracking on the mural. (d) Plaster Disruption: A state of looseness in the mural plaster layer caused by the action of soluble salts.

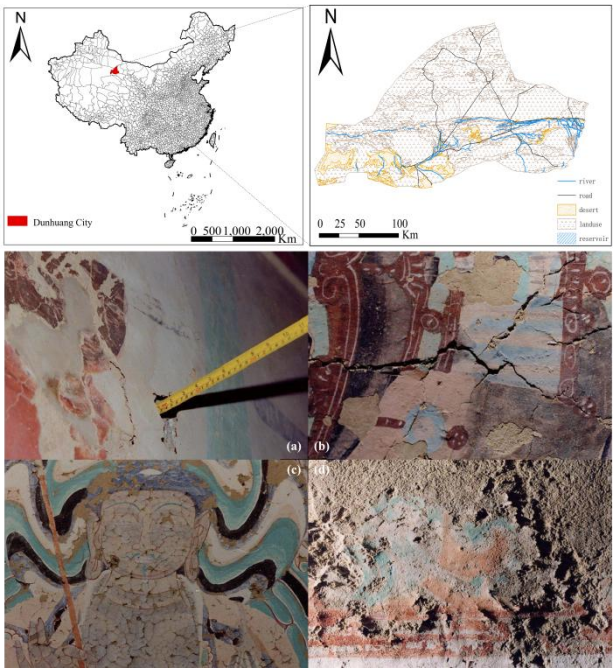

Figure 1. (a)- (c) depict an overview of the research area. (d) showcases typical pathological types found in mural paintings of the study area: (i)Salt efflorescence, (ii)Alkaline effervescence, (iii) Fissures, (iv) Crazing.

The methodology for sample preparation was informed by the study conducted by Bi (Bi,W. 2022), while the desalination process adheres to the GB/T50123-2019 standard. Frist, the raw materials—kaolinite clay, sand, and wheat straw—undergo a desalination process to eliminate potential interference from salts present in the original materials on the experimental outcomes. The procedure entails sieving a certain amount of dried soil sample through a 0.56 mm sieve, mixing it with deionized water in a 1:5 ratio, and stirring clockwise for 0.5 hours to dissolve the salts. Subsequently, the mixture is allowed to settle for 24 hours. After the supernatant water clears, it is removed, and this desalination process is repeated a total of five times. The effectiveness of the desalination is assessed by measuring the electrical conductivity of the soil sample, ensuring the total salt content does not exceed 0.1%. Following desalination, the soil sample is dried, crushed, and sieved for later use. Then, kaolinite clay, sand, and wheat straw are mixed in a 64:36:3 ratio, and distilled water equal to 20% of the solid mass is added. The uniformly mixed materials are filled into pre-greased molds, with the surface smoothed and excess air removed by vibration. Finally, the molds are placed in an oven at 90°C to dry, reducing the moisture content of the samples as much as possible to closely approximate a completely dry state. This series of preparatory steps is designed to fabricate mural plaster samples that meet experimental requirements, facilitating subsequent studies on the effects of salt damage.

3. DATA SOURCE AND METHODOLOGY

3.1 Data Collection

To investigate the hyperspectral characteristics of mural plaster in response to phosphate concentration, this experiment devised solutions of disodium hydrogen phosphate dodecahydrate at five different concentrations: 0.608, 0.808, 1.008, 1.208, and 1.408 mol/L, representing a range from the lowest to the highest erosion conditions. A high-precision, low-temperature constant temperature water bath was employed for temperature

control of the samples, maintaining a constant temperature of 32.5°C to simulate capillary absorption effects eroding the mural plaster samples(A total of 70 sets of samples, 14 samples under each working condition). After the samples were air-dried, their spectral reflectance was determined using an ASD-FieldSpec 4 Hi-Res spectroradiometer, collecting hyperspectral data. The wavelength range spanned from 350 to 2500 nm, with sampling intervals of 1.4 nm (350–1000 nm) and 2 nm (1001–2500 nm). To avoid the influence of other light sources, measurements were conducted under indoor, enclosed conditions devoid of external light sources at night. After a 30-minute instrument warm-up and standard reflectance calibration, the device's 57 optical fibers were embedded into an ASDP analytical (Model: A122317) high-brightness contact probe light source, a 70W quartz-tungsten-halogen lamp with an aperture diameter of 25mm. The light aperture was inverted directly above the center surface of the sample, the light source was activated, and upon stabilization of the curve, data was collected. The probe was then rotated 90° parallel to the sample surface to repeat the collection in four directions, followed by another measurement of the sample's center point, with the average value taken as the sample's spectral data, all within a darkroom.

To minimize the interference of salt content in the raw materials on the experimental outcomes, a desalination process was conducted on the raw materials. The phosphate content in the eroded mural samples was assessed by changes in electrical conductivity, with specific steps to measure conductivity as follows: In the laboratory, the mural samples post-phosphate erosion were sieved through a 2 mm soil sieve. A soil leachate was prepared at a 1:5 soil-to-water ratio and filtered at an indoor temperature of 25 °C. The soil leachate's electrical conductivity (EC) was measured using a soil salinity EC conductivity meter.Figure 2 presents the flowchart for sample preparation and the collection process of hyperspectral data for mural plaster.

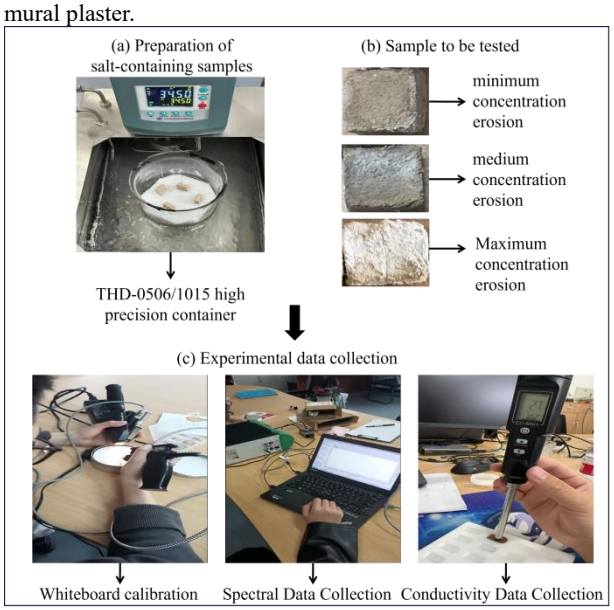

Figure 2.Preparation of samples and collection of hyperspectral data for Mural Plaster.

3.2 Statistical Analysis of Electrical Conductivity Data in Mural Plaster

The coefficient of variation is employed to articulate the degree of relative fluctuation or dispersion in conductivity measurement values.The electrical conductivity data of Mural Plaster collected under the five different conditions were statistically described using data density distribution, mean, standard deviation (SD), minimum value (Min), first quartile (Q1), third quartile (Q3), and coefficient of variation (CV). The first and third quartiles (Q1 and Q3) are indicated with red dashed lines, while the mean is denoted with a blue dashed line. OC1 to OC5 represent the five conditions ranging from minimal to maximal concentration erosion. The coefficient of variation (CV), also known as the dispersion coefficient, is a standardized measure of the dispersion of a probability distribution, defined as the ratio of the data's standard deviation to its mean. Data is considered to have low concentration variability when CV ≤ 15%, moderate variability when 15% < CV ≤ 35%, and high variability when CV > 35%. The formula for calculating the coefficient of variation (CV) is as follows(J. Zhang, et al. 2023):

$$CV = \frac{\sigma}{u} \times 100\% \tag{1}$$

where CV = the coefficient of variation (expressed as a perc entage)
σ = the standard deviation of the sample
u = the mean value of the sample

3.3 Preliminary Processing of Hyperspectral Data

Initially, the spectral reflectance data for mural plasters was cleansed of low signal-to-noise ratio bands between 350-399nm and 2401-2500nm. Following this, the Savitzky-Golay filter was applied to smooth the hyperspectral reflectance data of 100 simulated plaster layer samples(J. Chen, et al. 2004), utilizing 21 window points and a second-order polynomial (Guo Zhouqian, et al. 2023).

$$y_i^{'} = \frac{1}{\Delta} \sum_{j=-m}^{m} c_j \cdot y_{i+j} \tag{2}$$

where $y_i^{'}$ = the spectral reflectance at position i after smoothi ng.
y_{i+j} = points within the original data series.
c_j = coefficients in the convolution kernel, acquired t hrough polynomial fitting.
m = half the size of the window.
Δ = hypically 1, unless the intervals between data poi nts are non-uniform.

3.4 Research Methodology

3.4.1 Grünwald-Letnikov Fractional Differentiation

Fractional Order Differentiation (FOD) represents an extension of traditional integer-order differentiation and manifests in various forms within the realms of mathematics and engineering (Karaca, Yeliz, and Dumitru Baleanu. 2022), such as Riemann-Liouville (R-L), Lévy, Weyl, Caputo, and Grünwald-Letnikov (G-L) (Wang, X et al. 2020). The current experiment employs the Grünwald-Letnikov method, which, owing to its discrete nature, is particularly suitable for the numerical computation of hyperspectral signals (Equation 3),Γdenotes the Gamma function ($\Gamma(v) = (v-1)!$).

$$d^v f(x) = \lim_{h \to 0} \frac{1}{h^v} \sum_{n=0}^{[(t-a)/h]} (-1)^n \frac{\Gamma(v+1)}{n!\,\Gamma(v-n+1)} f(x - nh) \tag{3}$$

where v = the fractional order
h = step size
t and a = upper and lower bounds of FOD

In this experiment, assuming the function f (x) as a one-

dimensional hyperspectral signal with a band range of [a, t], where x ∈ [a, t] divided by the differential step length h. Given that the ASD FieldSpec® 3 Hi-Res Spectrometer's retention interval is 1nm, the differential step length can be set to h=1. Consequently, the expression for the v-th order fractional differentiation of the function f (x) can be derived from Equation (3) as follows(Wang,X et al. 2018):

$$\frac{d^{v} f(x)}{dx^{v}} \approx f(x) + (-v) f(x-1) + \frac{(-v)(-v+1)}{2} f(x-2) + \frac{(-v)(-v+1)(-v+2)}{6} f(x-3) + \ldots + \frac{\Gamma(-v+1)}{n!\,\Gamma(-v+n+1)} f(x-n) \tag{4}$$

where v = the fractional order
x = the wavelength

3.4.2 Construction of the Spectral Reflectance Index In recent years, numerous studies have focused on estimating soil components through spectral indices, particularly by employing dual-band spectral indices. These indices facilitate the elucidation of both the external responses and intrinsic meanings of spectral data, and they are capable of amplifying the subtle correlations between bands. Concurrently, the Phosphate Simple Ratio (PSR) and the Phosphate Normalized Difference Index (PNDI) place the strongest and weakest reflection bands in the numerator and denominator, respectively. Through operations of ratios and normalized ratios, they further expand the disparity between bands to maximize the sensitivity of the measured property attributes. The constructions of the PSR index and the PNDI index are represented by Equation 5 and Equation 6, respectively.

$$PSR = \frac{R_a}{R_b} \tag{5}$$

$$PNDI = \frac{R_a - R_b}{R_a + R_b} \tag{6}$$

Where R_a and R_b = denote the spectral reflectance at a given wavelength.

In this study, we introduce a novel three-band index—Phosphate Three Simple Ratio (PTSR)—aimed at enhancing the precision of spectral index estimates and bolstering their resistance to interference, thereby improving the monitoring of phosphate content in mural plaster. Further, by analyzing the best-performing spectral indices from the univariate regressions up to the sixth order, these indices were utilized as explanatory variables in a Partial Least Squares Regression (PLSR) analysis of ground phosphate content. In the accuracy comparison between the PSR-PLSR and PNDI-PLSR models, the best-performing model was selected as the basis for the three-band index study. Rc, denoting the waveband corresponding to the spectral index with the highest correlation coefficient with phosphate content, was incorporated as a specific sensitive waveband to further refine the spectral index design. The ultimately formulated three-band index, PTSR, is defined as Equation 7:

$$PTSR = \frac{R_a}{R_b - R_c} \tag{7}$$

Where R_a and R_b = represent the reflectance at specific wavebands a and b within the range of 400-2400 nm, respectively
R_c = denotes a particular waveband selected based on the optimal model.

3.4.3 Modeling PLSR In this study, univariate regression and Partial Least Squares (PLS) regression are employed to estimate the phosphate content in mural plaster. Univariate regression refers to a method involving only one independent variable and one dependent variable. For variable selection, the Pearson correlation coefficient is used to measure the strength of the linear relationship between the independent and dependent variables. This paper calculates the correlation coefficients between the PNDI, PSR, PTSR spectral indices, and the phosphate content in mural plaster. The absolute value of the correlation coefficient describes the degree of linear correlation between two variables. Consequently, this research selects the spectral index corresponding to the highest correlation coefficient as the independent variable, with the phosphate content in mural plaster as the dependent variable. The test and validation sets are split in a 7:3 ratio, conducting univariate regression to identify the optimal order and band position, providing a basis for establishing a multivariate regression model subsequently.To enhance the model's precision, data underwent standardization and mean centering as preprocessing steps. The model's framework is based on the Kernel PLS algorithm, with the number of principal components capped at seven. Optimal component numbers were determined through random cross-validation, and specific model warning parameters were set (thresholds for the calibration and validation residual variance ratio set at 0.5 and 0.75, respectively, and the upper limit for residual variance increase set at 6%) to ensure the model's stability and reliability.

In this study, the selection of specific three-band bands no longer simply relies on the outcomes of previous research but instead employs a data-driven analytical approach. The essence of this method lies in delving into the domain of fractional order differentiation, systematically identifying the most appropriate orders and band positions.

3.4.4 Evaluation This paper employs–accuracy assessment metrics to evaluate the efficacy of the predictive modeling (Tian, A et al. 2021;Zhang,J et al. 2023). The computation formulas for R^2, RMSE (Root Mean Square Error), and MAE (Mean Absolute Error) are delineated as follows in Equations (8) to (10).

$$R^2 = \left(\frac{\sum_{i=1}^{n} \left(y_i - \bar{y}\right)\left(z_i - \bar{z}\right)}{\sqrt{\sum_{i=1}^{n} \left(y_i - \bar{y}\right)^2 \cdot \sum_{i=1}^{n} \left(z_i - \bar{z}\right)^2}} \right)^2 \tag{8}$$

$$RMSE = \sqrt{\frac{\sum_{i=1}^{n} \left(y_i - z_i\right)^2}{n}} \tag{9}$$

$$MAE = \frac{1}{n} \sum_{i=1}^{n} \left| y_i - \hat{y}_i \right| \tag{10}$$

where n = the number of mural plaster samples
y_i = the EC measurement value of the *i*-th mural plaster sample

$\bar{y}$ = the average value of the measured values of all mural plaster samples

z_i = the predicted EC value of the i-th mural plaster sample

$\bar{z}$ = the average EC predicted value of all mural floor samples

The coefficient of determination of the calibration data set is expressed as R_c^2. The root mean square error of the calibration data set and the validation data set is expressed as $RMSE_c$ and $RMSE_v$. The coefficient of determination of the validation data set is expressed as R_v^2, and the performance of the model is expressed as MAE. Among them, R^2 is used to evaluate the model fitting degree. The closer the value is to 1, the higher the model accuracy. RMSE and MAE are used to evaluate the stability of the model. The closer the value is to 0, the better the RMSE and MAE are.

4. RESULTS

4.1 Statistical Description of Mural Plaster Electrical Conductivity

The electrical conductivity (EC) values of the mural plaster samples directly reflect the variance in salt content within the same material, exhibiting a certain degree of variability. As illustrated in Figure 3, the range of sample EC values spans from 2.20 ms·m^-1 to 4.86 ms·m^-1. The mean and standard deviation of the sample EC values are calculated to be 3.50 ± 0.76 ms·m^-1. The first quartile (Q1) and third quartile (Q3) of the data are respectively 2.92 ms·m^-1 and 4.15 ms·m^-1, indicating that 50% of the sample EC values fall between these two figures. Additionally, the coefficient of variation (CV) stands at 21%, signifying that the relative variability of the EC values is at a moderate level

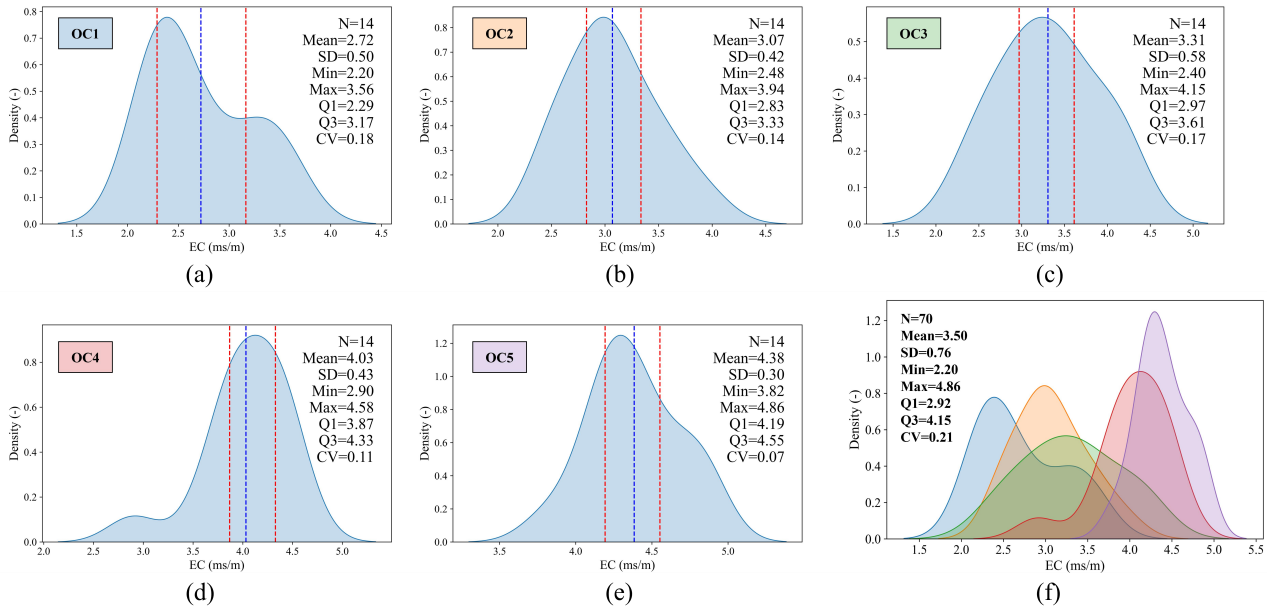

Figure 3.Statistical description of the Electrical Conductivity (EC) values in Mural Plaster.

4.2 Hyperspectral Characteristics of Simulated Mural Plaster under Different Salt Concentration Erosion

Based on Equation 2, the spectral data are smoothed to highlight these spectral features. As observed in Figure 4, the reflectance spectra of Mural Plaster, subjected to varying concentrations of salt erosion, exhibit similar shapes. The colored curve represents the average spectrum of the Mural Plaster samples. Within the 400-2400 nm wavelength range, shows reflectance values between 0.08 and 0.45, displaying notable fluctuations.

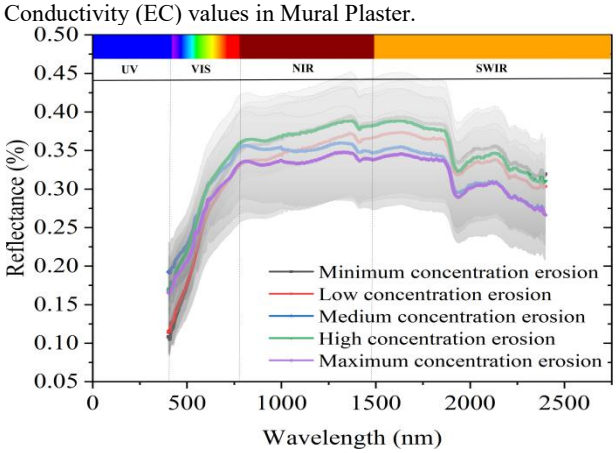

Figure 4. Spectral reflectance curves of mural samples under different conditions.

4.3 Fractional Order Differentiation Results of Spectral Curves

Given the rich high-dimensional information in hyperspectral data and the difficulty in capturing sensitive bands and features

(Song, G et al. 2023), the FOD calculation method delineated in Section 3.4.1 was utilized on the samples, employing Equation (4) to enhance the analysis. This method allows for the control of differential step length, thereby enhancing the accuracy of salt content detection. Following the approach of (Zhang,J et al. 2023), the interval and step length were set at [0-2] and 0.1, respectively. Figure 7 illustrates the average spectrum of the Mural Plaster samples.

After treatment with FOD, the Mural Plaster samples exhibited three distinct hygroscopic troughs near 1400nm, 1900nm, and 2200nm, indicative of enhanced water absorption characteristics. This enhancement is associated with an increase in both porosity and surface roughness of the samples following phosphate treatment, thereby augmenting their water-absorptive capacity. As the stages of FOD treatment progressed, a decline in the spectral curve profiles was observed. At the 0.5 stage, the reflectance corresponding to the full spectral wavelength fluctuated primarily between 0 and 0.03, beginning to show negative values; by the 0.8 stage, the reflectance had already fallen below 0.1. Following the 0.6 differential spectrum stage, substantial, readily observable fluctuations in the curves emerged, amplifying differences between the spectral lines. However, increasing the stage did not allow for further expansion of these differences, and from stage 1.1 onward, this trend gradually slowed. After stage 1.4, the spectral curve profiles became blurred and superimposed, indicating that at higher order differentials, the profiles of the spectral curves are progressively obscured, and the distinct intervals between the curves are lost.

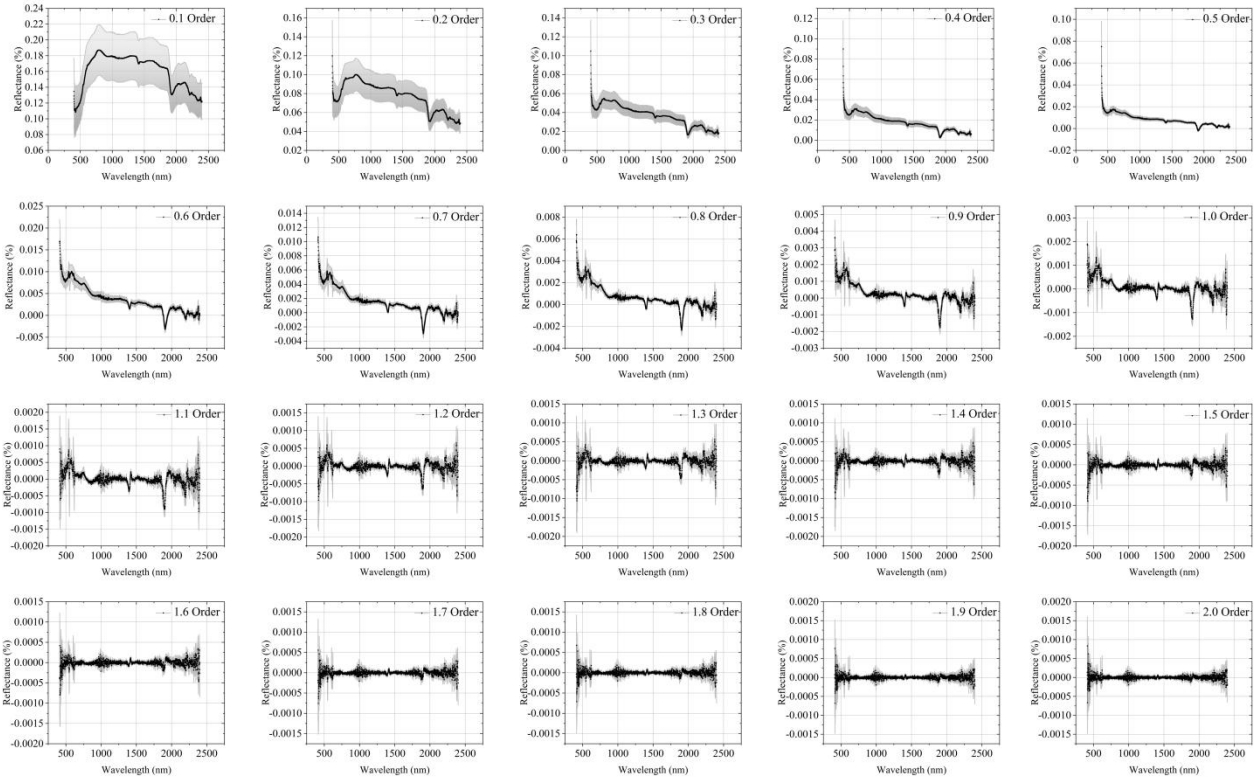

Figure 5. Average fractional-order derivative spectra of Mural Plaster samples. The range of orders spans from 0 to 2, with a step size of 0.1. Colored curves represent the average spectra of Mural Plaster samples, while the gray shadow indicates their standard deviation.

4.4 Spectral index analysis

From Table 1, it can be observed that the Maximum Absolute Correlation Coefficient (MACC) between PNDI and phosphate content exhibits a trend of initial increase followed by a decrease with the advancing stages of FOD treatment. Notably, at the 0.6 stage, the MACC reaches its peak value of 0.652, indicating that at this stage, FOD treatment is most effective in enhancing the correlation between PNDI and phosphate content.We can observe the performance of linear regression models based on the two-band spectral index (PNDI) across various stages of FOD treatment. The analysis encompasses FOD stages including 0.3, 0.8, 0.2, 0.4, 0.9, and 1.2, with these stages ranking among the top six in model accuracy out of all the stages tested.

Order	MACC	R_a (nm)	R_b (nm)	Calibration Dataset			Validation Dataset		
				R_c^2	$RMSE_c$	MAE_c	R_v^2	$RMSE_v$	MAE_v
0.1	0.6	862	846	0.567	0.461	0.392	0.645	0.466	0.395
0.2	0.625	887	844	0.57	0.457	0.377	0.698	0.417	0.373
0.3	0.613	886	841	0.509	0.487	0.409	0.728	0.394	0.312
0.4	0.593	894	825	0.578	0.464	0.39	0.667	0.406	0.321
0.5	0.627	879	825	0.592	0.455	0.376	0.537	0.463	0.399
0.6	0.652	879	825	0.627	0.452	0.378	0.601	0.422	0.334
0.7	0.628	879	824	0.587	0.466	0.384	0.544	0.472	0.377
0.8	0.626	401	449	0.677	0.365	0.28	0.699	0.495	0.439
0.9	0.624	401	462	0.477	0.489	0.389	0.655	0.455	0.368
1	0.579	798	770	0.47	0.522	0.457	0.437	0.515	0.455
1.1	0.625	1407	847	0.563	0.471	0.408	0.507	0.495	0.43
1.2	0.596	1407	815	0.4	0.51	0.446	0.651	0.518	0.48
1.3	0.587	2186	1051	0.47	0.506	0.432	0.39	0.499	0.423
1.4	0.582	401	1370	0.479	0.502	0.416	0.53	0.482	0.41
1.5	0.566	401	1370	0.519	0.481	0.405	0.47	0.518	0.422
1.6	0.549	1369	403	0.493	0.485	0.401	0.357	0.581	0.513
1.7	0.557	402	1764	0.496	0.498	0.419	0.393	0.588	0.511
1.8	0.555	401	1764	0.38	0.511	0.434	0.559	0.575	0.506
1.9	0.559	401	1764	0.39	0.507	0.432	0.556	0.577	0.495
2	0.532	401	1409	0.461	0.504	0.429	0.437	0.534	0.465

Table 1. Employing linear regression, we have derived the estimation results for the characteristic wavelengths of phosphate content in Mural Plaster and the Two-Band Spectral Index (PNDI)

Table 2 reveals that the Maximum Absolute Correlation

Coefficient (MACC) between PSR and phosphate content also exhibits a trend of initial increase followed by a decrease with the progression of FOD stages, mirroring the trend observed with PNDI. Notably, at stage 0.6, the MACC reaches its apex at 0.653. Further in-depth analysis using the data presented in Table 2 indicates that when employing the single two-band spectral index (PSR) for model construction, the 0.3 stage of Fractional Order Derivative (FOD) processing achieves the highest determination coefficient (R^2 = 0.728), significantly enhancing the accuracy of phosphate content estimation. Moreover, a comparative analysis of FOD treatments from stages 0.1 to 0.8 versus 1 to 2 reveals that lower-order derivatives (0.1 to 0.8 stages) are more effective in estimating phosphate content.

Order	MACC	R_a (nm)	R_b (nm)	Calibration Dataset			Validation Dataset		
				R_c^2	$RMSE_c$	MAE_c	R_v^2	$RMSE_v$	MAE_v
0.1	0.601	846	862	0.567	0.461	0.392	0.645	0.466	0.396
0.2	0.625	844	887	0.57	0.457	0.377	0.698	0.417	0.373
0.3	0.613	841	886	0.509	0.487	0.409	0.728	0.394	0.312
0.4	0.598	427	481	0.54	0.465	0.378	0.626	0.485	0.419
0.5	0.627	879	825	0.591	0.456	0.377	0.538	0.463	0.399
0.6	0.653	879	825	0.627	0.452	0.378	0.604	0.420	0.333
0.7	0.630	401	449	0.607	0.398	0.306	0.728	0.457	0.383
0.8	0.633	401	449	0.678	0.365	0.279	0.700	0.494	0.441
0.9	0.624	918	879	0.616	0.448	0.371	0.452	0.526	0.442
1	0.599	750	848	0.455	0.492	0.420	0.597	0.539	0.475
1.1	0.629	748	848	0.579	0.465	0.393	0.459	0.571	0.442
1.2	0.567	1403	848	0.499	0.499	0.419	0.490	0.537	0.466
1.3	0.587	401	1370	0.556	0.465	0.378	0.457	0.529	0.442
1.4	0.582	401	1370	0.478	0.502	0.417	0.530	0.482	0.409
1.5	0.755	402	1394	0.246	0.609	0.521	0.270	0.574	0.496
1.6	0.567	491	2049	0.434	0.518	0.445	0.339	0.558	0.465
1.7	0.556	402	1764	0.494	0.499	0.420	0.391	0.589	0.513
1.8	0.555	401	1764	0.379	0.511	0.434	0.559	0.575	0.506
1.9	0.559	401	1764	0.390	0.507	0.432	0.556	0.577	0.495
2	0.558	401	1764	0.396	0.504	0.431	0.540	0.587	0.506

Table 2. Employing linear regression, we have derived the estimation results for the characteristic wavelengths of phosphate content in Mural Plaster and the Two-Band Spectral Index (PSR)

The correlation coefficients between the three-band spectral indices at various FOD stages and the phosphate content in Mural Plaster are depicted in Figure 6 and Table 3. The horizontal and vertical axes represent spectral bands. Table 3 lists the Maximum Absolute Correlation Coefficients (i.e., the greatest value among the maximum positive and negative correlation coefficients). Employing a cumulative comparative method, the Maximum Absolute Correlation Coefficient for the three-band spectral indices increased by 5.32% compared to PSR, indicating that the adoption of a three-band combination for fractional order derivative processing substantially enhances the correlation between the spectral indices and phosphate content.

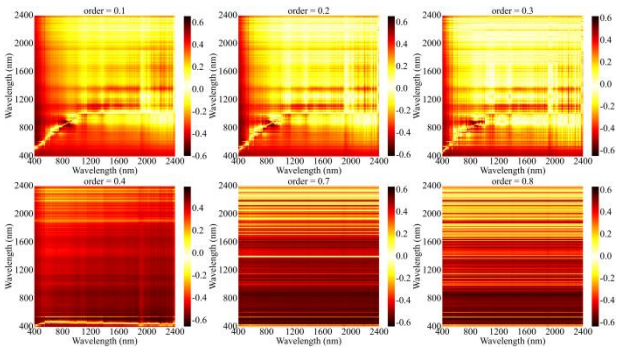

Figure 6. Correlation Coefficient Between Phosphate Content in Mural Plaster and the Three-Band Spectral Index (PTSR)

Order	MACC	R_b (nm)	R_h (nm)	R_v (nm)	Calibration Dataset			Validation Dataset		
					R_c^2	$RMSE_c$	MAE_c	R_v^2	$RMSE_v$	MAE_v
0.1	0.653	815	836	846	0.627	0.427	0.364	0.73	0.417	0.336
0.2	0.65	815	829	844	0.631	0.427	0.365	0.653	0.423	0.368
0.3	0.654	957	904	841	0.553	0.476	0.392	0.557	0.491	0.437
0.4	0.66	2194	482	427	0.508	0.455	0.366	0.767	0.441	0.356
0.7	0.639	2057	449	401	0.615	0.394	0.305	0.753	0.436	0.364
0.8	0.641	2057	449	401	0.687	0.360	0.277	0.722	0.476	0.423

Table 3. Employing linear regression, we have derived the estimation results for the characteristic wavelengths of phosphate content in Mural Plaster and the Two-Band Spectral Index (PTSR).

4.5 Predictive Model for Phosphate Content in Mural Plaster Based on Fractional Order Differential Combined with Novel Spectral Indices

In this study, we employed Fractional Order Derivative (FOD) technology and the three-band spectral index (PTSR) to develop a high-precision model for monitoring phosphate content in Mural Plaster. Figure 7 presents the optimal model for Mural Plaster phosphate monitoring constructed using FOD spectra and the PTSR index (based on validation set data). The color bar in the figure represents the density of data points, determined through Gaussian Kernel Density Estimation (KDE), where darker regions indicate higher densities of data points, and lighter regions signify lower densities. Upon detailed analysis, the PTSR-PLSR model demonstrated a significant enhancement in performance compared to the previous PNDI-PLSR and PSR-PLSR models, specifically achieving a coefficient of determination (R^2) of 0.815 and reducing the root mean square error (RMSE) to 0.327, an improvement of 10.4% and 7.38% in accuracy, respectively. These results not only confirm the high accuracy and reliability of the PTSR-PLSR model in monitoring the phosphate content of Mural Plaster but also highlight the potential of FOD technology and the innovative three-band spectral index in the field of hyperspectral remote sensing.

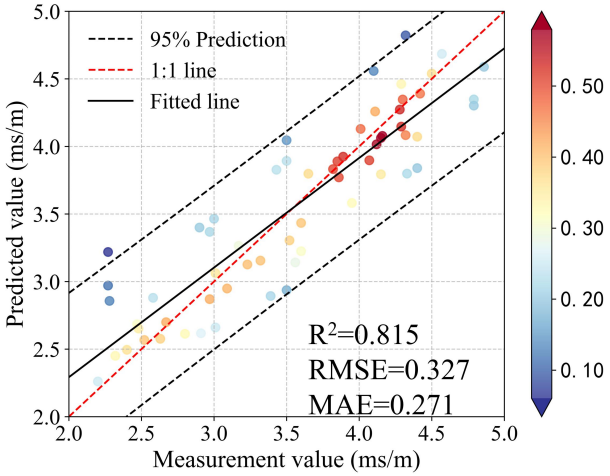

Figure 7. The Optimal Mural Plaster Phosphate Monitoring Model Established Based on FOD Spectra and Three-Band Spectral Index (PTSR) Using Validation Set Data

5. DISUSSION

The innovations of this study are as follows:

(1) In this research, we have developed an innovative three-band spectral index, named the Phosphate Three Simple Ratio (PTSR). This index is designed to enhance the accuracy of estimations and to augment resistance to environmental interferences, thereby optimizing the monitoring of phosphate content in Mural Plaster

(2)The research has developed a model combining Fractional Order Differentiation and Partial Least Squares Regression (PTSR-FOD-PLSR) for the hyperspectral feature inversion of Mural Plaster phosphate content. This enables non-destructive

detection and accurate prediction of phosphate content in Dunhuang Mural Plaster, which holds significant value for cultural heritage conservation.

However, it is pertinent to acknowledge the limitations of this study. The limitations of this study are primarily manifested in several areas: Firstly, although the efficacy of the Phosphate Three Simple Ratio (PTSR) three-band spectral index has been demonstrated to surpass that of the two-band PNDI and PSR indices, a comprehensive cross-comparison of different model construction forms (such as normalization, quadratic, logarithmic, exponential, etc.) with specific research subjects has not been conducted, thereby restricting a thorough understanding of the factors influencing model precision. Furthermore, the potential of machine learning methods to enhance computational efficiency has not been fully explored, which may hinder advancements in the processing and analysis of hyperspectral data. Moreover, although the Partial Least Squares Regression (PLSR) model has proven effective, insufficient exploration of its analogous alternative methods has limited the possibilities for model optimization and innovation. Lastly, the effectiveness of the research methodologies has not been further validated through field tests using hyperspectral cameras. Future research directions will focus on addressing these limitations, particularly through field testing to deeply explore the performance of hyperspectral cameras under complex field conditions; systematic comparative analysis of different three-band spectral index construction forms to identify the most suitable model types; and seeking effective alternatives to Partial Least Squares Regression to optimize existing models, thereby enhancing their accuracy and practicality. These research directions not only aim to overcome the present limitations but also to advance the application of hyperspectral technology in soil composition monitoring and other fields.

6. CONCLUSION

This research successfully developed a hyperspectral characteristic inversion model for the quantification of phosphate content in Mural Plaster, utilizing a novel three-band spectral index in conjunction with Fractional Order Differential and Partial Least Squares Regression algorithms. This model offers an efficient and precise method for non-invasive, non-destructive salt damage monitoring, overcoming various limitations associated with traditional methodologies, such as high costs, low efficiency, and potential physical damage risks.

REFERENCES

Sun, Tongxin, et al., 2023: Restoring Dunhuang Murals: Crafting Cultural Heritage Preservation Knowledge into Immersive Virtual Reality Experience Design.*International Journal of Human–Computer Interaction*., 1-22. doi.org/10.1080/10447318.2023.2232976

Sharma, Anjali, Manager Rajdeo Singh, and Rajat Jangid., 2023: Scientific study of the pigments and binders used in mural painting from the 16th-century ce St Mary's Church of Cheriapally, Kottyam, Kerala, and its relevance to conservation.*Archaeometry* 65.3 617-634. doi.org/10.1111/arcm.12836.

Li D.,Hu Q.,Ruan S.,et al. 2023: Utilizing Hyperspectral Reflectance and Machine Learning Algorithms for Non-Destructive Estimation of Chlorophyll Content in Citrus Leaves. *Remote Sensing.*, 15 (20): 4934. doi.org/10.1021/10.3390/rs15204934.

Peng W.,Beggio G.,Pivato A.,et al. 2022: Applications of near infrared spectroscopy and hyperspectral imaging techniques in anaerobic digestion of bio-wastes: A review. *Renewable and Sustainable Energy Reviews.*, 165: 112608. doi.org/10.1016/j.rser.2022.112608.

Schodlok M C.,Frei M,Segl K., 2022: Implications of new hyperspectral satellites for raw materials exploration. *Mineral Economics.*, 35 (3-4): 495-502. doi.org/10.1007/s13563-022-00327-

Ma J.,Zheng B.,He Y. 2022: Applications of a hyperspectral imaging system used to estimate wheat grain protein: A review. *Frontiers in Plant Science.*, 13: 837200. doi.org/10.3389/fpls.2022.837200.

Zhang, Z.; Ding, J.; Wang, J.; Ge, X., 2020: Prediction of soil organic matter in northwestern China using fractional-order derivative spectroscopy and modified normalized difference indices.*Catena.*2020,185,104257.doi.org/10.1016/j.catena.2019.104257.

Noda, I., 2006: Progress in two-dimensional (2D) correlation spectroscopy. *Journal of Molecular Structure.* 2006, 799, 2-15. doi.org/10.1016/j.molstruc.2006.03.053.

Chen, L.; Lai, J.; Tan, K.; Wang, X.; Chen, Y.; Ding, J., 2022: Development of a soil heavy metal estimation method based on a spectral index: Combining fractional-order derivative pretreatment and the absorption mechanism.*Science of the Total Environment.*2022,813,151882.doi.org/10.1016/j.scitotenv.2021.151882.

Yuan, J.; Gao, J.; Yu, B.; Yan, C.; Ma, C.; Xu, J.; Liu, Y.,2024: Estimation of soil organic matter content based on spectral indices constructed by improved Hapke model. *Geoderma.* 2024, 443, 116823. doi.org/10.1016/j.geoderma.2024.116823.

Bi,W. 2022: Study on coupled heat and mass transfer process and characteristics of earthen plasters in Mogao Grottoes. *Doctor,Xi’an University of Architecture and Technology.*, doi.org/10.27393/d.cnki.gxazu.2022.000010.

J. Chen, P. Jönsson, M. Tamura, Z. Gu, B. Matsushita, and L. Eklundh. 2004: A simple method for reconstructing a high-quality NDVI time-series data set based on the Savitzky–Golay filter. *Remote sensing of Environment*. 91, 332-344, doi.org/10.1016/j.rse.2004.03.014.

Guo Zhouqian.,Lv Shuqiang.,et al. 2023: Inversion of salt content in simulated mural based on Hyperspectral mural salt index.*Spectroscopy and Spectral Analysis.*, 43 (10): 3272-3279. doi.org/10. 3964/j.issn.1000-0593 (2023)10-3272-08.

Karaca, Yeliz, and Dumitru Baleanu. 2022: Evolutionary Mathematical Science, Fractional Modeling and Artificial Intelligence of Nonlinear Dynamics in Complex Systems.*Chaos Theory and Applications* 4.3 111-118.

Wang,X., Zhang,F., Kung,H. T., Johnson,V. C., Latif,A., 2020: Extracting soil salinization information with a fractional-order filtering algorithm and grid-search support vector machine (GS-SVM) model.*International Journal of Remote Sensing*,41 (3),953-973. doi.org/10.1080/01431161.2019.1654142.

Tian,A., Zhao,J., Tang,B., Zhu,D., Fu,C., Xiong,H., 2021: Hyperspectral prediction of soil total salt content by different disturbance degree under a fractional-order differential model with differing spectral transformations.*Remote Sensing*., 13 (21),4283. doi.org/10.3390/rs13214283.

Zhang, J., Jing, X., Song, X., Zhang, T., Duan,W., Su, J., 2023: Hyperspectral estimation of wheat stripe rust using fractional order differential equations and Gaussian process methods.*Computers and Electronics in Agriculture.*,206, 107671. doi.org/10.1016/j.compag.2023.107671.